INTERNATIONAL JOURNAL OF CLIMATOLOGY
Int. J. Climatol. **26**: 1895–1912 (2006)
Published online 3 May 2006 in Wiley InterScience
(www.interscience.wiley.com) DOI: 10.1002/joc.1341

RMetS
ROYAL METEOROLOGICAL SOCIETY

TROPICAL PACIFIC AND SOUTH ATLANTIC EFFECTS ON RAINFALL VARIABILITY OVER NORTHEAST BRAZIL

RITA VALÉRIA ANDREOLI* and MARY TOSHIE KAYANO
Instituto Nacional de Pesquisas Espaciais, Centro de Previsão de Tempo e Estudos Climáticos, Avenida dos Astronautas, 1758, 12227-010 São José dos Campos, SP, Brasil

Received 17 May 2005
Revised 23 February 2006
Accepted 4 March 2006

ABSTRACT

The present paper reexamines the relative role of the tropical Pacific and tropical South Atlantic (TSA) on the rainfall over Northeast Brazil (NEB). For several variables, El Niño-Southern Oscillation (ENSO) and TSA-related anomalous patterns are obtained. These patterns are then compared to the combined ENSO and TSA-related patterns to infer the relative importance of the two oceanic basins on the rainfall over NEB. Analyses are done for austral summer and autumn seasons. Considering the composite technique, six cases are examined: El Niño and neutral conditions in the TSA, La Niña and neutral conditions in the TSA, ENSO neutral conditions and warm TSA, ENSO neutral conditions and cold TSA, El Niño and warm TSA, and La Niña and cold TSA. The most important result comes from the cases with competing influences of the tropical Pacific and the TSA. In some of these cases, the SST variability in the TSA is the determining factor of the NEB climate. The result of this study might be useful mainly for regional climate monitoring purposes. Copyright © 2006 Royal Meteorological Society.

KEY WORDS: ENSO; Tropical South Atlantic; rainfall anomalies; Northeast Brazil

1. INTRODUCTION

El Niño-Southern Oscillation (ENSO) in the tropical Pacific is the main remote influence for climate variations over Northeast Brazil (NEB). This connection occurs through changes in the atmospheric circulation in such a way that, under El Niño conditions, the Walker circulation is eastward displaced, with its ascending branch situated in the eastern equatorial Pacific where the convection is enhanced, and its descending branch situated over NEB and the adjacent tropical Atlantic (TA) where the convection is inhibited (Hastenrath, 1976; Kousky *et al*., 1984; Kayano *et al*., 1988; Ropelewski and Halpert, 1987, 1989; Kiladis and Diaz, 1989).

On the other hand, strong relations between the NEB rainfall and the sea-surface temperature (SST) anomalies in the TA have been documented in several papers (Hastenrath and Heller, 1977; Moura and Shukla, 1981; Hastenrath, 1990; Hastenrath and Greischar, 1993; Nobre and Shukla, 1996). Modeling and observational studies have shown that these relations occur through associations between the SST anomalies in the TA and the meridional displacements of the Atlantic Intertropical Convergence Zone (ITCZ) (Hastenrath and Heller, 1977; Moura and Shukla, 1981). The dominant pattern of the TA variability mode is characterized by coherent zonally symmetric anomalies of SST, surface wind, and net surface heat flux organized in the meridional direction (Nobre and Shukla, 1996; Seager *et al*., 2001). This variability has been attributed to the ocean–atmosphere interactions with a positive feedback between the surface heat flux and the SST anomalies (Chang *et al*., 1997). The cross equatorial SST gradient affects the location of the ITCZ, which in turn affects the NEB rainfall variability. The seasonal meridional excursion of the Atlantic ITCZ into the Southern

* Correspondence to: Rita Valéria Andreoli, Instituto Nacional de Pesquisas Espaciais, Centro de Previsão de Tempo e Estudos Climáticos, Avenida dos Astronautas, 1758, 12227-010 São José dos Campos, SP, Brazil; e-mail: rita@cptec.inpe.br

Copyright © 2006 Royal Meteorological Society

WILEY InterScience®
DISCOVER SOMETHING GREAT

Hemisphere (SH) might be delayed during the NEB rainy season (from March to May – MAM) owing to the presence of positive SST anomalies in the Tropical North Atlantic (TNA), thus resulting in droughts in the NEB. Conversely, the presence of positive SST anomalies in the Tropical South Atlantic (TSA) favors the southward displacement of the ITCZ, which in extreme cases might cause floods.

However, the TA SST variability, in particular in its northern sector, has strong dependence on the tropical Pacific climate variability. ENSO-related atmospheric anomalies are responsible for changes in the strength of the TNA trade winds during the SH summer. These winds drive the surface heat flux anomalies causing a local SST response in the TNA during the SH autumn, one season after the mature stage of ENSO extremes (Curtis and Hastenrath, 1995; Enfield and Mayer, 1997). Nobre and Shukla (1996) provided evidence showing that this process occurs through a midlatitude 'atmospheric bridge' resembling the Pacific-North American (PNA) teleconnection pattern, which ends up affecting the Atlantic ITCZ positioning. Thus, they proposed that ENSO, through the SST cross equatorial gradient, affects the Atlantic ITCZ position.

On the other hand, Giannini *et al.* (2004) suggested that the TA SST conditions during the development stage of ENSO extremes might precondition the development of ENSO-related teleconnections. They found strong relationship between the NEB rainfall and the TA SST variations when the same sign SST anomalies prevail in the eastern equatorial Pacific and in the TNA (concordant years). In this case, the NEB rainfall response to ENSO extremes is reinforced by the TA SST variability. Under opposite sign anomalies in the eastern equatorial Pacific and in the TNA (discordant years), the NEB rainfall anomaly pattern, which can be even the reverse of that related to ENSO, is determined by the TA SST variability. Pezzi and Cavalcanti (2001) obtained similar results using simulation data.

While some authors have provided evidence that ENSO relates to the NEB rainfall via the midlatitude atmospheric bridge, others have shown that this relationship might operate directly through an anomalous Walker circulation that influences the Atlantic ITCZ positioning (Saravanan and Chang, 2000; Giannini *et al.*, 2001; Chiang *et al.*, 2000).

SST variations in the tropical Pacific and in the TA play an important role in the NEB rainfall variability. One aspect, not addressed before, concerns the isolated effects of the tropical Pacific and the TA on the NEB rainfall. Since SST variations in the TNA are closely related to ENSO, the TSA SST variability is chosen in order to isolate the tropical Pacific and the TA effects on the NEB climate. The choice of the TSA is justified because it is as important as the TNA in generating the TA SST variability (Giannini *et al.*, 2004). Moreover, Kane (1992), using the SST indices defined by Servain (1991), provided evidence that Fortaleza rainfall variations have stronger relations to the southern than to the northern sector of the TA. So, this paper aims to analyze the role of the tropical Pacific and the TSA on rainfall over NEB. Isolated and combined effects of the SST variability in these two basins on the NEB rainfall are analyzed for the austral summer (from December to February - DJF) and autumn (MAM) seasons. The associated SST and atmospheric circulation patterns are also examined.

2. DATA AND METHODOLOGY

The data used here is monthly global gridded SST and sea-level pressure (SLP), respectively, at 2° by 2° and 5° by 5° latitude-longitude resolution grids. The SST data consists of the reconstructed SST (ERSST) for the 1854–2000 period obtained by Smith and Reynolds (2003). The SLP data is obtained from the British Atmospheric Data Center at the web page http://www.badc.rl.ac.uk/for the 1871–1994 period. Monthly reanalyzed 925 hPa wind, 200 hPa stream function (200 hPa ψ), and 500 hPa vertical velocity (500 hPa ω) data for the period from 1948 to 1999 are also used. This data was produced by the Climate Data Assimilation System (CDAS) Reanalysis Project (Kalnay *et al.*, 1996) and has a resolution of 2.5° in latitude and longitude. Monthly rainfall series in the South American area, bounded by the equator, 15 °S, 50 °W, and 30 °W, for the 1912–1999 period are extracted from several sources taking into account the availability of information for the period from 1912 to 1999. The sources of rainfall data are: the Superintendência do Desenvolvimento do Nordeste (SUDENE), the Instituto Nacional de Meteorologia (INMET), and the Agência Nacional de Energia Elétrica (ANEEL). Gridded rainfall series over NEB, selected from the 'gu23wld0098.dat'

Copyright © 2006 Royal Meteorological Society

DOI: 10.1002/joc

(version 1.0) constructed and provided by Dr Mike Hulme, are also used. A description of this data set can be found in Hulme (1992, 1994) and in Hulme *et al*. (1998). Prior to use, this data set was checked for errors. Monthly values higher than 2000 mm and suspicious values (detected by inspections of the series) were replaced by the missing data code. Figure 1 illustrates locations of the rainfall grid points and stations.

Monthly anomalies of variables at each grid point are obtained as departures from the 1912–1999 means for SST and rainfall, from the 1912–1994 means for SLP and from the 1948–1999 means for the reanalyzed variables. The SLP, SST, and rainfall anomaly series at each grid point are standardized by the corresponding standard deviation of the anomaly time series. The standardized SST anomalies at each grid point are linearly detrended. In order to emphasize the wave-like structure in the 200 hPa ψ anomaly fields, the zonal means are removed from the anomaly series of this variable.

Selection of ENSO extremes is based on the observed Niño-3 index, defined as the averaged SST anomalies in the area bounded at 6°N, 6°S, 150°W, and 90°W. An El Niño (A La Niña) event is identified when the December–February means of the Niño-3 SST index exceeds (is lower than) the threshold of 0.9 °C (–0.7 °C). The absolute threshold for cold events is smaller than that for warm events to compensate unbalanced intensities of El Niño and La Niña events reflected in the Niño-3 index.

A monthly index representing the SST variability in the TSA is obtained by averaging the SST anomalies in the region delimited by the equator, 20°S, 30°W, and 10°E. As far as the combined as well as the isolated effects of ENSO and of TSA SST variability on the NEB rainfall are concerned, warm and cold events in the TSA (WTSA and CTSA) are selected considering the seasonal means of the SST index for DJF. A WTSA (CTSA) event is selected when the SST anomaly index is above (below) one standard deviation ($\sigma = 0.26$ °C). The neutral TSA is referred to as NTSA. Table I lists the years with El Niño/La Niña and WTSA/CTSA events occurring simultaneously/separately for the period 1912–1999. Cases with simultaneous occurrences of El Niño (La Niña) and CTSA (WTSA) are not analyzed because their numbers are too low to perform composites. It is worthwhile to note that the establishment of positive (negative) SST anomalies in the TNA for strong El Niño (La Niña) events (Saravanan and Chang, 2000) does not necessarily imply the establishment of opposite sign SST anomalies in the TSA.

The years listed in Table I are based on DJF anomaly time series. Composites are done for these selected DJF seasons and for the following MAM seasons. Prior to calculating the composites, the seasonal (DJF and MAM) averages of monthly anomalies are obtained. These composites are for rainfall anomalies over NEB, for SST anomalies in the area bounded by 60°N, 60°S, 120°E, and 30°E, for SLP and 200 hPa ψ anomalies in the global band between 80°N and 80°S, and for other variable anomalies in the area bounded by 40°N, 40°S, 80°W, and 30°E. Composites using reanalyzed data provide only an approximate idea of the associated circulation patterns because they are based on the cases for the 1948–1999 period.

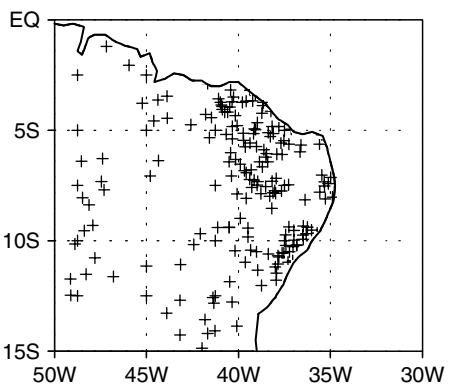

Figure 1. Locations of the rainfall grid points and stations

Copyright © 2006 Royal Meteorological Society

DOI: 10.1002/joc

Table I. Years with El Niño/La Niña and WTSA/CTSA events occurring simultaneously/separately for the 1912–1999 period

El Niño, WTSA	El Niño, NTSA	La Niña, CTSA	La Niña, NTSA	ENSO Neutral, WTSA	ENSO Neutral, CTSA
1940–41	1913–14	1942–43	1916–17	1915–16	1917–18
1951–52	1918–19	1954–55	1922–23	1920–21	1921–22
1972–73	1925–26	1955–56	1924–25	1923–24	1929–30
1982–83	1930–31	1975–76	1949–50	1934–35	1950–51
1997–98	1941–42	1996–97	1967–68	1945–46	1953–54
–	1957–58	–	1970–71	1963–64	1959–60
–	1986–87	–	1973–74	1983–84	1969–70
–	1991–92	–	1984–85	1987–88	1977–78
–	–	–	1988–89	1994–95	1980–81
–	–	–	1998–99	–	–

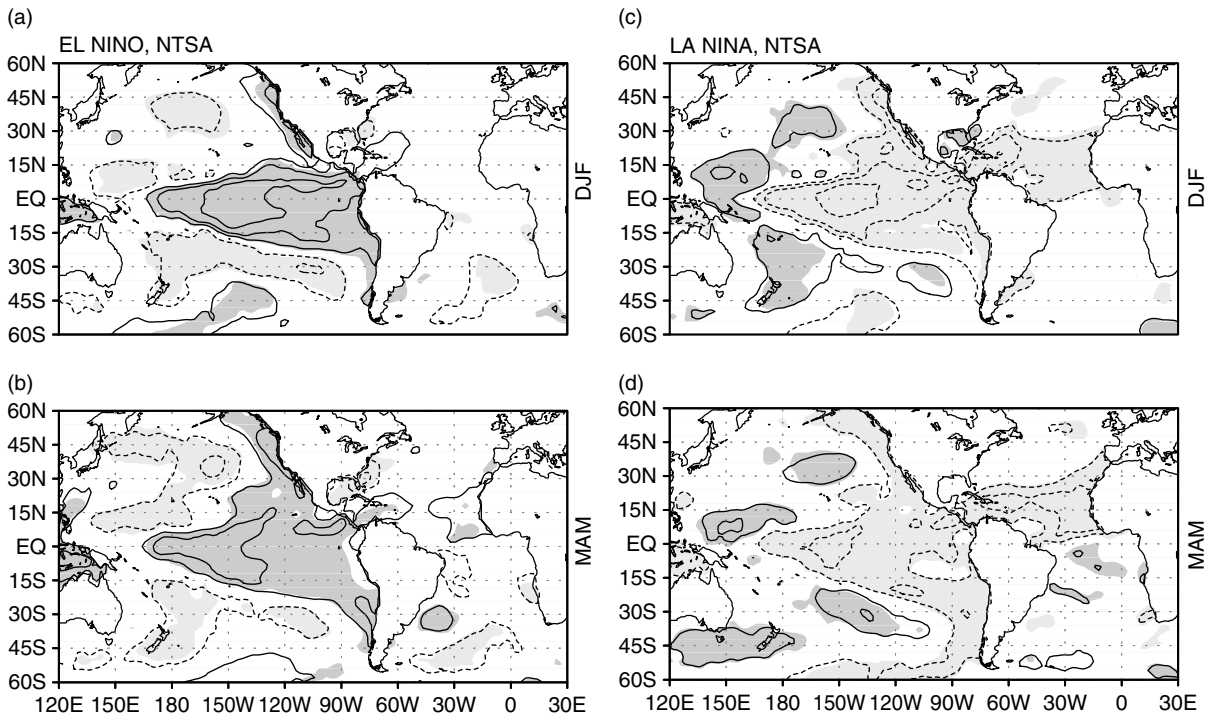

Figure 2. Mean standardized SST anomalies for El Niño and NTSA during (a) DJF and (b) MAM; mean standardized SST anomalies for La Niña and NTSA during (c) DJF and (d) MAM. The zero line is omitted. Contour interval is 0.5 standard deviations with negative (positive) contours being dashed (continuous). Shaded area encompasses significant values at the 95% confidence level

Statistical significance of the composites is assessed assuming that the number of degrees of freedom is the number of events. It is assumed that a variable X with n values and S standard deviation shows a Student-t distribution. So, only the composites with absolute values exceeding $t_{\alpha(n-1)}S/\sqrt{(n-1)}$ are statistically significant (Panofsky and Brier, 1968). The confidence level of 95% is used.

Copyright © 2006 Royal Meteorological Society

DOI: 10.1002/joc

3. RESULTS

3.1. Tropical Pacific influence

As expected, the SST anomaly composites for El Niño and La Niña events under NTSA conditions show approximately reversed sign patterns in the Pacific region for both the analyzed seasons (Figure 2). El Niño (La Niña) composites present positive (negative) SST anomalies along the west coast of the Americas and in the central and eastern equatorial Pacific flanked to the north and to the south by opposite sign significant anomalies. The SST anomaly patterns for DJF resemble the SST anomaly patterns previously obtained during the mature stage of canonical El Niño events (Rasmusson and Carpenter, 1982). For both seasons, El Niño composites show quite small anomalies in the TA, and La Niña composites present significant negative anomalies in an extensive area of the TNA. The TA SST anomaly pattern represents a southward SST gradient, which has been related to La Niña events in previous papers (Enfield and Mayer, 1997; Saravanan and Chang, 2000).

Figure 3 displays the associated composites for SLP anomalies. For this variable, El Niño and La Niña composites present approximately reversed sign zonal wave number one structure in the tropics during DJF (Figure 3(a) and (c)). Indeed, one center is noted in the eastern hemisphere (the largest anomalies in the Australasian region) and opposite sign center in the western hemisphere (a center in the central tropical Pacific). The zonal wave number one structure for the tropical SLP anomalies resembles the austral summer ENSO-related SLP anomaly mode obtained in previous papers (Kayano and Kousky, 1993; Kayano and Andreoli, 1998). For El Niño composites, significant negative SLP anomalies are also found over North America with the largest amplitudes in the Aleutian low-pressure system region during DJF (Figure 3(a)). For La Niña composites, significant positive anomalies are scattered in the central North Pacific and to the south of 40 °S (in the South Atlantic and the Indian Ocean) during DJF (Figure 3(c)). In MAM, the SLP

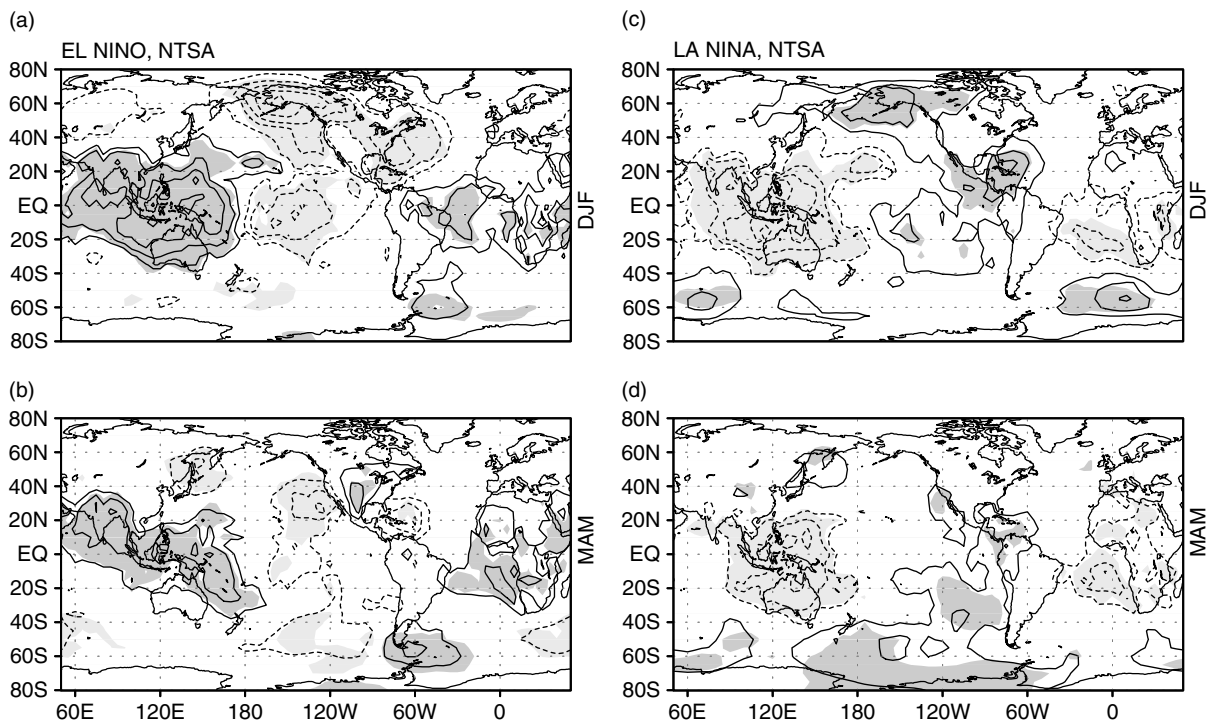

Figure 3. Mean standardized SLP anomalies for El Niño and NTSA during (a) DJF and (b) MAM; Mean standardized SLP anomalies for La Niña and NTSA during (c) DJF and (d) MAM. Contour interval is 0.3 standard deviations with negative (positive) contours being dashed (continuous). Shaded area encompasses significant values at the 95% confidence level

Copyright © 2006 Royal Meteorological Society

DOI: 10.1002/joc

anomalies are weakened in the northern midlatitudes and less extensive in the tropics than those during DJF for El Niño and La Niña composites. In MAM, significant SLP anomalies are also found in the central Pacific between 40 °S and 60 °S (negative), in the southwest Atlantic (positive) for El Niño composites (Figure 3(b)), and in the southern Pacific (positive) for La Niña composites (Figure 3(d)). The consistency between SLP and SST anomalies is more conspicuous in the tropical Pacific for El Niño composites and in the tropical Pacific and TA for La Niña composites. The anomalous northward SLP gradient in the TA for La Niña composites is coherent with the presence of negative SST anomalies in the TNA for both seasons.

Figure 4 shows the associated 200 hPa stream function anomaly patterns. As for the other variables, El Niño and La Niña composites of the 200 hPa stream function anomalies show approximately reversed sign patterns (Figure 4). El Niño composites of the 200 hPa ψ anomaly present three pairs of dipoles straddling the equatorial latitudes with the first pair in the central equatorial Pacific (anticyclonic circulations), the second one in the equatorial Atlantic (cyclonic circulation), and the third pair (the weakest one) in the western Pacific and Indonesian region (cyclonic circulations). These circulation centers in both hemispheres are centered at 20° in latitude (Figure 4). In the eastern tropical Pacific, the region with the largest SST anomalies (Figure 2), the Rossby wave pattern for the 200 hPa ψ extends from central Pacific to midlatitudes of both hemispheres and resembles the PNA pattern in the Northern Hemisphere (NH) (Horel and Wallace, 1981) and the Pacific/South America (PSA) pattern in the SH (Mo, 2000; Mo and Nogués-Paegle, 2001). The intensities of the northern and southern branches of the Rossby wave patterns depend on the ENSO phase and on the season. While the NH branches weaken, the SH branches strengthen from DJF to MAM for both ENSO phases. The dipolar structures in the equatorial Pacific and the equatorial Atlantic strengthen from DJF to MAM for both ENSO phases.

For El Niño (La Niña) composites, the pair of upper-level anticyclones (cyclones) in the central equatorial Pacific accompanying heated (cooled) surface waters (Figures 2 and 4) implies rising (descending) motion

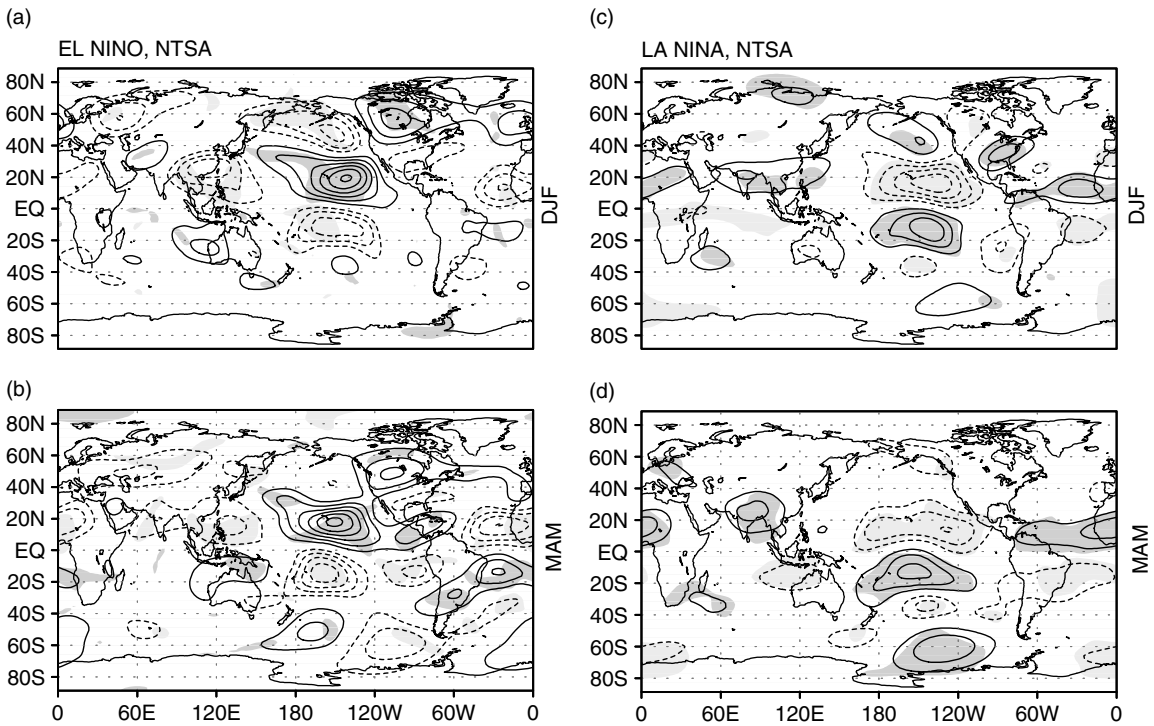

Figure 4. Composites of the 200 hPa ψ anomalies for El Niño and NTSA during (a) DJF and (b) MAM; composites of the 200 hPa ψ anomalies for La Niña and NTSA during (c) DJF and (d) MAM. Contour interval is $2.0 \times 10^{+6}$ m^2/s with negative (positive) contours being dashed (continuous). The zero line is omitted. Shaded area encompasses significant values at the 95% confidence level

Copyright © 2006 Royal Meteorological Society

DOI: 10.1002/joc

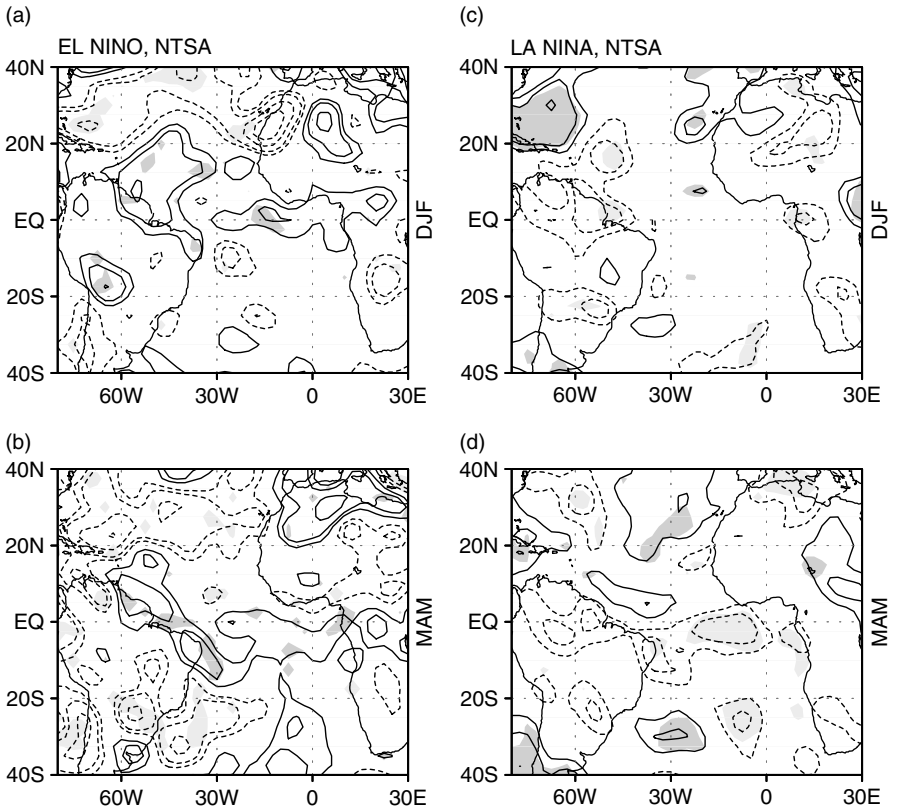

Figure 5. Composites of the 500 hPa ω anomalies for El Niño and NTSA during (a) DJF and (b) MAM; composites of the 500 hPa ω anomalies for La Niña and NTSA during (c) DJF and (d) MAM. Contour interval is 0.01 Pa/s with negative (positive) contours being dashed (continuous). The zero line is omitted. Shaded area encompasses significant values at the 95% confidence level

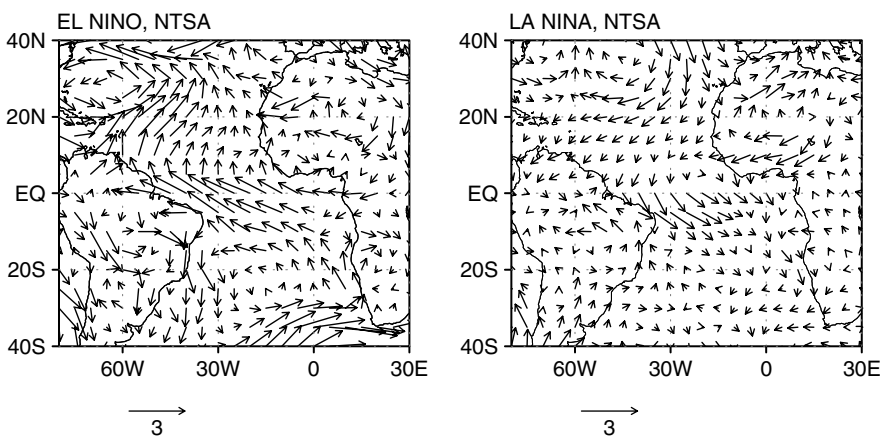

Figure 6. Composites of the 925 hPa anomalous wind vectors during MAM for (a) the El Niño and NTSA and (b) for La Niña and NTSA. Arrows at the bottom of each panel illustrate the base magnitude of the wind vector in m/s

in this region and compensating descending (rising) motions over TSA and NEB (Figure 5). In fact, the associated 500 hPa ω anomaly patterns present descending (ascending) motions over NEB for El Niño (La Niña) composites. The 500 hPa ω anomalies show a slight intensification from DJF to MAM (Figure 5).

Copyright © 2006 Royal Meteorological Society

DOI: 10.1002/joc

Therefore, deficient (excessive) rainfall over NEB for El Niño (La Niña) composites during both seasons is expected.

In order to infer the low-level wind characteristics for ENSO extremes and NTSA conditions, composites of the 925 hPa wind are obtained for MAM (Figure 6). The northeast trades are weaker (stronger) than normal when the surface waters in the central Pacific are anomalously warm (cold). El Niño (La Niña) composites also show an anomalous flow across the ITCZ climatological position with strong southeasterly (northwesterly) winds in the equator–10 °S latitudinal band, which is consistent with a northward (southward) SST gradient in the TA. Thus, these anomalous low-level wind and SST fields suggest an anomalously northern (southern) positioning of the ITCZ, which justifies the observed droughts (floods) over NEB for El Niño (La Niña) composites (Figure 7). The wind patterns in the TA are consistent with previous results on ENSO-related atmospheric anomalies (Curtis and Hastenrath, 1995; Enfield and Mayer, 1997).

The rainfall anomaly composites feature approximately reversed sign patterns for the two ENSO phases. For El Niño (La Niña) composites during DJF, negative (positive) anomalies are found in the northern sector of the NEB, and opposite sign anomalies to the south (Figure 7(a) and (c)). The rainfall anomalies for this season might be attributed primarily to ENSO-related atmospheric teleconnections featuring a global rearrangement of air mass by means of a zonal seesaw in SLP. This is due to the fact that ENSO-remote SST response in the TNA is only starting to build up during DJF (Enfield and Mayer, 1997). During MAM, the rainfall anomalies occupy most of NEB with significant values over its northern sector (Figure 7(b) and (d)). These anomalies might be associated with ENSO-related atmospheric bridge and with ENSO-remote SST response in the TNA. This is due to the fact that the SH autumn usually marks the period of transition from ENSO to normal atmospheric conditions and the period when a delayed TNA SST response to ENSO becomes significant (Enfield and Mayer, 1997; Saravanan and Chang, 2000). The SST anomalous patterns in the TNA during MAM are highly consistent with previous findings on ENSO's relationship to the TA variability (Enfield and Mayer, 1997; Saravanan and Chang, 2000).

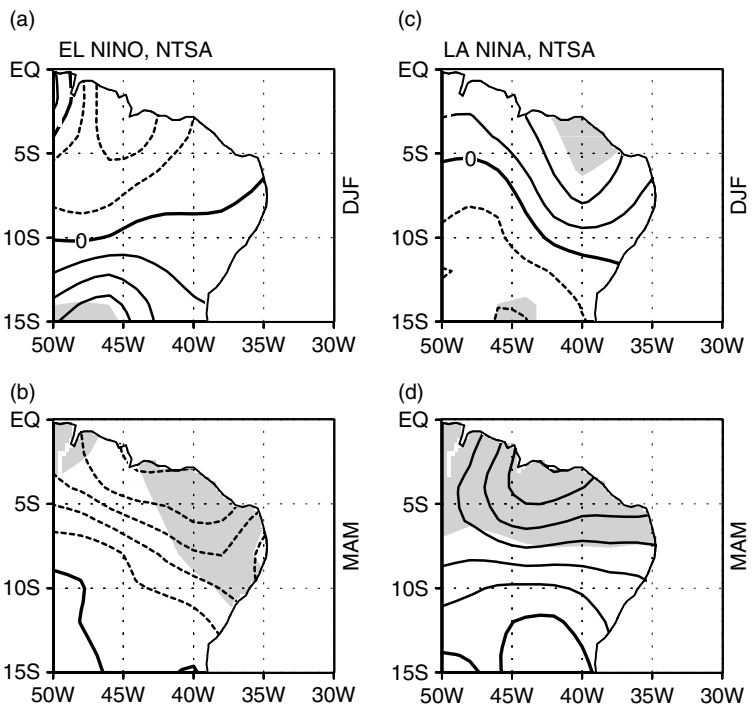

Figure 7. Mean standardized rainfall anomalies for El Niño and NTSA during (a) DJF and (b) MAM; mean standardized rainfall anomalies for La Niña and NTSA during (c) DJF and (d) MAM. Contour interval is 0.2 standard deviations, with negative (positive) contours being dashed (continuous). Shaded area encompasses significant values at the 90% confidence level

Copyright © 2006 Royal Meteorological Society

DOI: 10.1002/joc

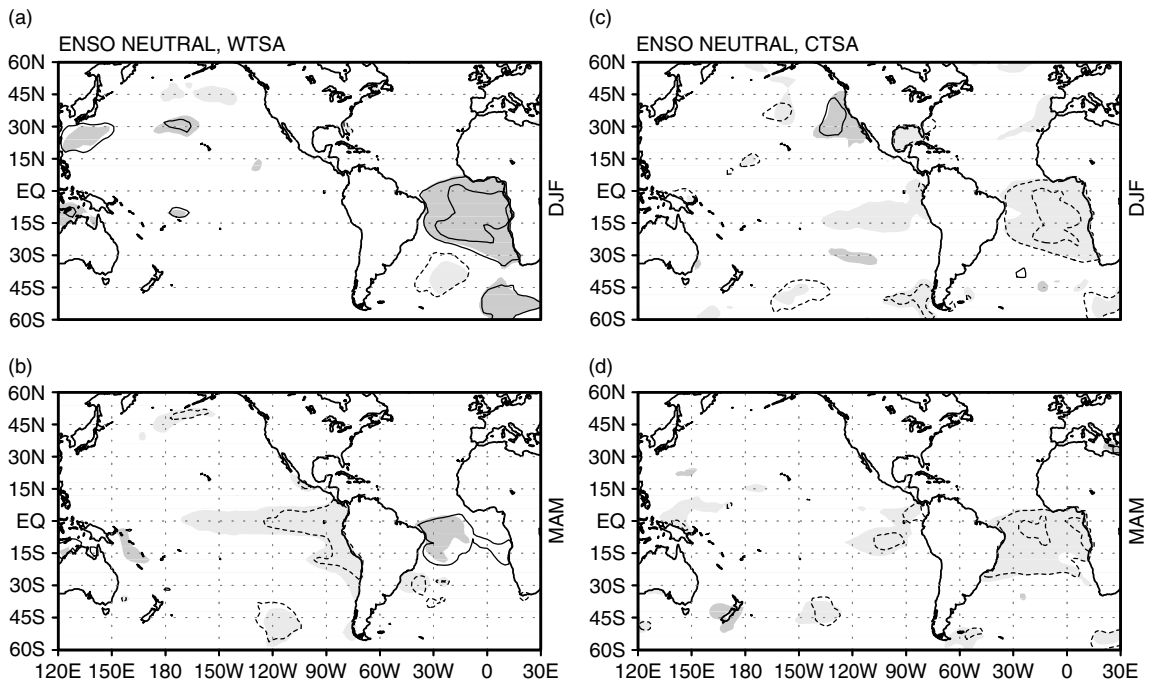

Figure 8. Mean standardized SST anomalies for ENSO neutral conditions and WTSA during (a) DJF and (b) MAM; mean standardized SST anomalies for ENSO neutral conditions and CTSA during (c) DJF and (d) MAM. Display is the same as that in Figure 2. Shaded area encompasses significant values at the 95% confidence level

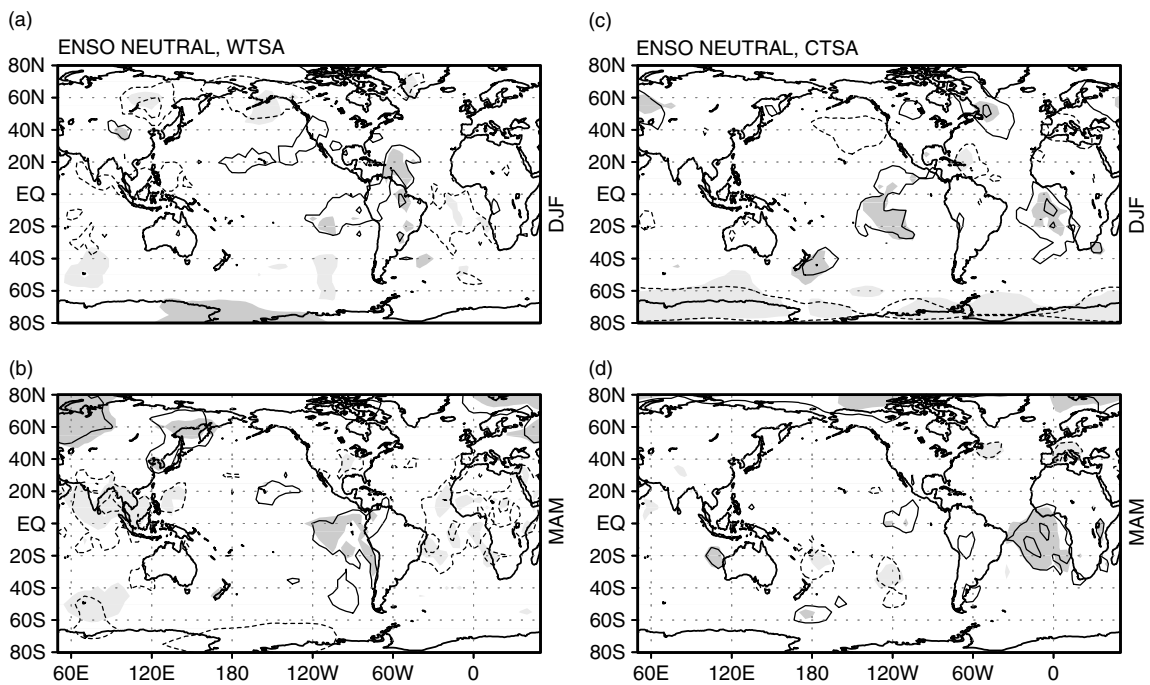

Figure 9. Mean standardized SLP anomalies for ENSO neutral conditions and WTSA during (a) DJF and (b) MAM; mean standardized SLP anomalies for ENSO neutral conditions and CTSA during (c) DJF and (d) MAM. Display is the same as that in Figure 3. Shaded area encompasses significant values at the 95% confidence level

Copyright © 2006 Royal Meteorological Society

DOI: 10.1002/joc

3.2. Tropical south Atlantic influence

The SST anomaly composites for WTSA and CTSA events under ENSO neutral conditions are displayed in Figure 8. These composites show approximately reversed sign patterns, in particular during DJF. In this season, positive (negative) anomalies are found over equatorial Atlantic and in most of the TSA for the WTSA (CTSA) composite. The WTSA composite also presents significant negative anomalies centered at (35 °S, 20 °W) during DJF, which practically disappear in MAM (Figure 8(a) and (b)). For the CTSA composite, the negative SST anomalies in the equatorial Atlantic and in the TSA weaken from DJF to MAM (Figure 8(c) and (d)). Weak negative SST anomalies are noted in the eastern equatorial Pacific for the WTSA composite during MAM.

The associated SLP anomaly patterns show significant values mostly in the tropics (Figure 9). The WTSA (CTSA) composite features negative (positive) SLP anomalies in the TSA and positive (negative) ones in the Caribbean Sea during DJF. In MAM, the CTSA composite presents strengthened positive SLP anomalies in the equatorial TA and TSA (Figure 9). In MAM, significant SLP anomalies are found in the eastern equatorial Pacific (positive) and in the equatorial TA (negative) for the WTSA composite. The positive SLP anomalies in the eastern equatorial Pacific are consistent with the presence of negative SST anomalies in this region during MAM (Figure 8(b)). The positive SLP anomalies in the eastern equatorial Pacific and negative ones in the equatorial Atlantic imply strengthened regional east/west circulation for the WTSA composite.

The associated composites of the 500 hPa ω show quite consistent patterns. The WTSA composites present hints of ascending motions over equatorial Atlantic and NEB, and of descending motions in the western TNA (Figure 10(a) and (b)). The ascending motions over equatorial Atlantic are consistent with

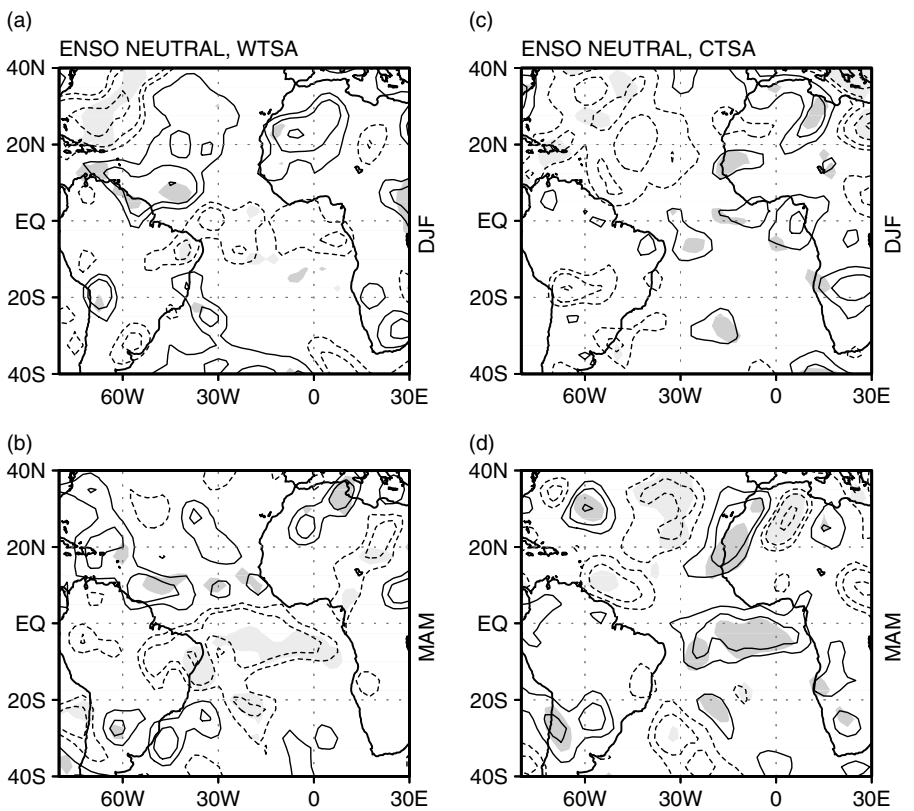

Figure 10. Composites of the 500 hPa ω anomalies for ENSO neutral conditions and WTSA during (a) DJF and (b) MAM; composites of the 500 hPa ω anomalies for ENSO neutral conditions and CTSA during (c) DJF and (d) MAM. Display is the same as that in Figure 5. Shaded area encompasses significant values at the 95% confidence level

Copyright © 2006 Royal Meteorological Society

DOI: 10.1002/joc

the presence of warmer than normal surface waters and below normal SLP in this region (Figures 8(a), (b), 9(a) and (b)). The CTSA composite shows ascending motions to the north of 5°N and hints at descending motions in the equatorial Atlantic during DJF (Figure 10(c)). In MAM, the CTSA composite features ascending motions in the TNA and descending motions along the northwest coast of Africa and in the eastern equatorial Atlantic (Figure 10(d)). The descending motions in the eastern equatorial Atlantic are consistent with the negative SST anomalies and positive SLP anomalies in this same region (Figures 8(d) and 9(d)).

The associated composites of the 925 hPa wind anomalies are displayed in Figure 11. The WTSA composite for DJF shows an anomalous anticyclonic circulation center in the central TNA approximately at 35°N, a strong anomalous cyclonic circulation center to the south of 20°S, and anomalous cross equatorial northwesterlies (Figure 11(a)). This cross equatorial flow shows the largest magnitudes in the equator–10°S latitudinal band. This pattern is indicative of an anomalously intensified subtropical high-pressure system in the TNA and weakened subtropical high-pressure system in the TSA. The anomalous low-level northwesterlies at the equatorial band displace the ITCZ toward the underlying heated regions of the equatorial Atlantic and TSA. On the other hand, the weakened subtropical high-pressure system in the TSA is consistent with the positive SST anomalies in the equatorial Atlantic and TSA (Figures 8(a) and 11(a)). This weakened subtropical high-pressure system yields a weakened Benguela current, thus the equatorward transport of cold surface

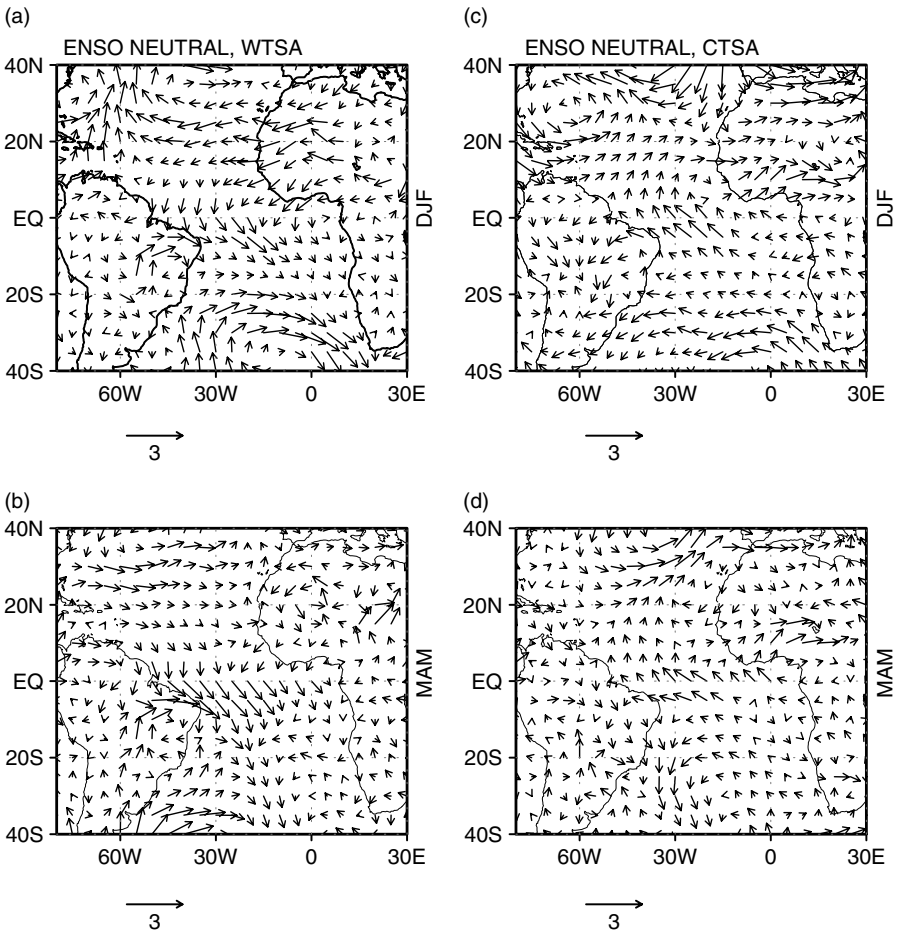

Figure 11. Composites of the 925 hPa anomalous wind vectors for ENSO neutral conditions and WTSA during (a) DJF and (b) MAM; composites of the 925 hPa anomalous wind vectors for ENSO neutral conditions and CTSA during (c) DJF and (d) MAM. Arrows at the bottom of each panel illustrate the base magnitude of the wind vector in m/s

Copyright © 2006 Royal Meteorological Society

DOI: 10.1002/joc

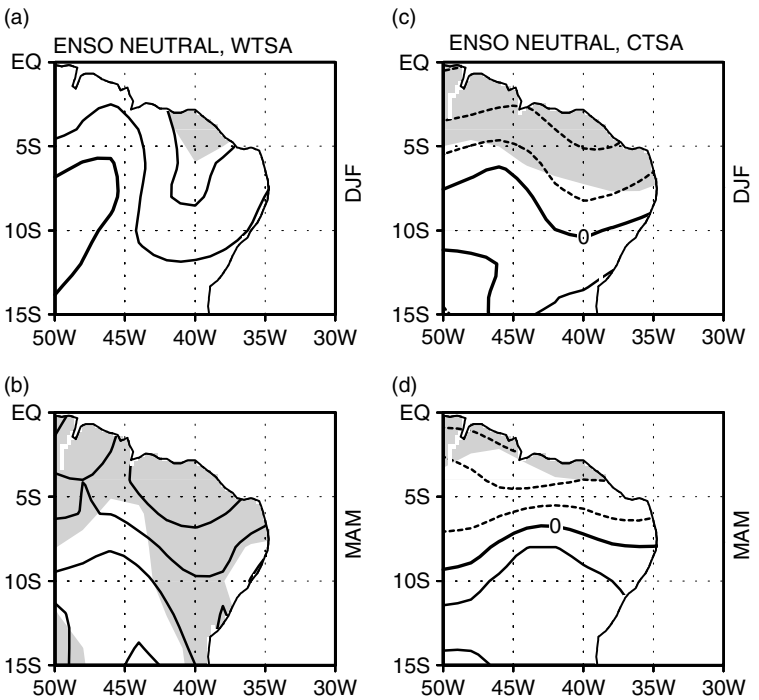

Figure 12. Mean standardized rainfall anomalies for ENSO neutral conditions and WTSA during (a) DJF and (b) MAM; mean standardized rainfall anomalies for ENSO neutral conditions and CTSA during (c) DJF and (d) MAM. Display is the same as that in Figure 7. Shaded area encompasses significant values at the 90% confidence level

waters from higher latitudes is also reduced. Consequently, positive SST anomalies are established in the equatorial latitudes (Figure 8(a)). In MAM, the anomalous low-level northwesterlies at the equatorial band (Figure 11(b)) maintain the ITCZ to the south of its normal position. This favors the occurrence of positive NEB rainfall anomalies (Figure 12(b)). The CTSA composites of the 925 hPa wind (Figures 11(c) and (d)) show nearly reversed circulation patterns to those of the WTSA composites (Figures 11(a) and (b)). The strengthened subtropical high-pressure system in the TSA is consistent with negative SST anomalies in the equatorial Atlantic and TSA (Figures 8(c), (d), 11(c) and (d)). In this case, the intensified southeasterlies in the equatorial Atlantic and along the NEB coast and the negative SST anomalies in the equatorial TA and in the TSA inhibit the southward displacement of the ITCZ during DJF and MAM. This explains the reduction in area of significant rainfall anomalies, which remain along the northern coast of NEB for the CTSA composites (Figures 12(c) and (d)).

3.3. Simultaneous influences of the tropical Pacific and TSA

The SST anomaly composites for El Niño and WTSA (warm composites) and for La Niña and CTSA (cold composites) are displayed in Figure 13. The warm composites feature positive SST anomalies in the central and eastern Pacific, in the equatorial TA, and in most of the TSA during DJF (Figure 13(a)). The negative (or southward) cross equatorial SST anomaly gradient in the TA contrasts with the expected warming of the surface waters in the TNA associated with an El Niño event (Enfield and Mayer, 1997). In MAM, the SST anomalies weaken in the Pacific and in the Atlantic sectors, but hints of positive anomalies remain in the eastern equatorial Pacific and in the TSA (Figure 13(b)). For the cold composites, the negative SST anomalies in the central and eastern Pacific, in the equatorial TA, and in most of the TSA are flanked to the south by positive SST anomalies during DJF (Figure 13(c)). In MAM, the negative SST anomalies weaken in the eastern equatorial Pacific but remain quite strong in the TSA (Figure 13(d)). The positive (or northward) cross equatorial SST anomaly gradient in the TA conflicts with the expected cooling of the surface waters in

Copyright © 2006 Royal Meteorological Society

DOI: 10.1002/joc

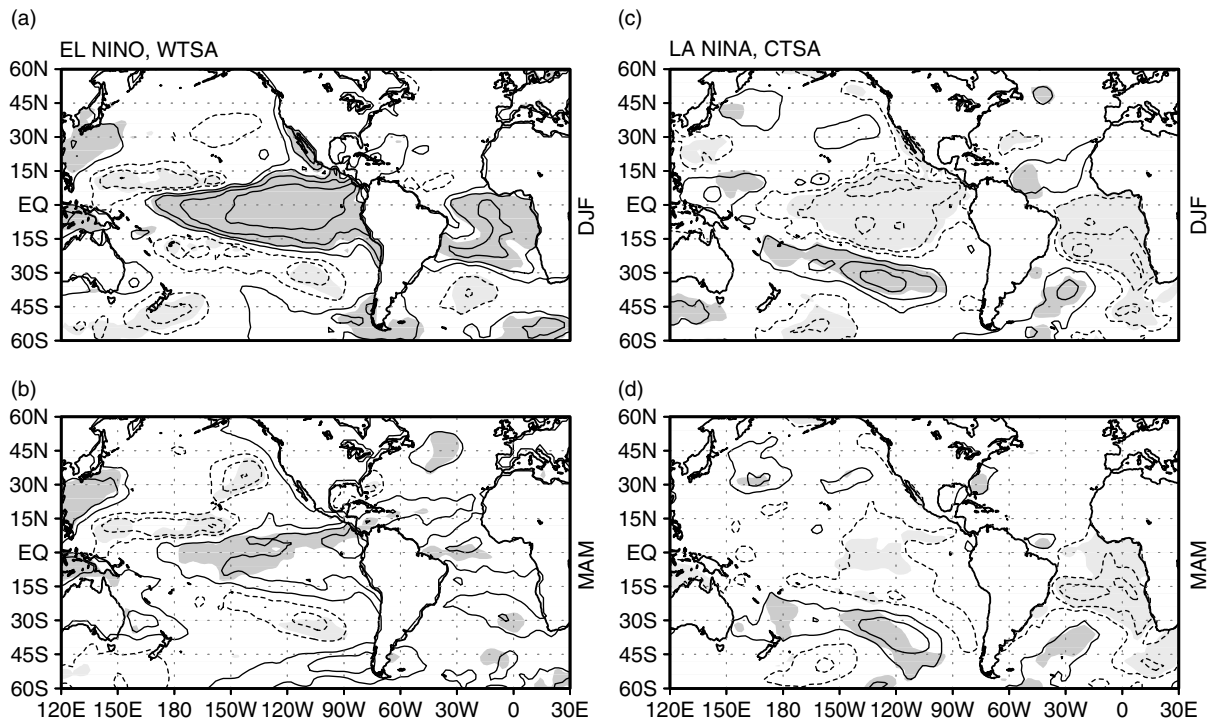

Figure 13. Mean standardized SST anomalies for El Niño and WTSA during (a) DJF and (b) MAM; mean standardized SST anomalies for La Niña and CTSA during (c) DJF and (d) MAM. Display is the same as that in Figure 2. Shaded area encompasses significant values at the 95% confidence level

the TNA associated with a La Niña event (Enfield and Mayer, 1997). For both cold and warm composites, the SST anomalous patterns in the eastern equatorial Pacific and in the TSA independently have opposite effects on the NEB rainfall.

The associated composites of the SLP anomalies are presented in Figure 14. The warm composite of the SLP anomalies shows significant positive values in the area extending from eastern Indian Ocean to western Pacific between the equator and 40 °S and in the eastern TA during DJF (Figure 14(a)). Weak (nonsignificant) negative anomalies are found in the central and eastern tropical Pacific and along the west coast of the Americas (Figure 14(a)). In MAM, significant positive SLP anomalies are found over western Pacific while the SLP anomalies are weakened elsewhere (Figure 14(b)). The cold composite of the SLP anomalies presents significant positive values in the central tropical Pacific and along the west coast of Mexico, and negative ones over Papua/New Guinea, northern Australia, Africa, and the adjacent TNA region during DJF (Figure 14(c)). In MAM, the cold composite of the SLP anomalies shows significant values only in small areas of the central Pacific and Central America. The significant SLP anomalies for warm and cold composites noted in the TNA and in the equatorial TA during DJF might illustrate the tropical component of ENSO teleconnection. On the other hand, the absence of significant SLP anomalies in most of the TA during MAM might result from the competing effects of the SST variability in the eastern tropical Pacific and in the TSA during DJF. El Niño (La Niña) remotely induces below (above) normal SLP anomalies in the TNA, which reach their maximum values during MAM (Covey and Hastenrath, 1978; Saravanan and Chang, 2000). Conversely, positive (negative) SST anomalies in the TSA induce above (below) normal SLP anomalies in the same region during MAM. As a consequence of these competing remotely and locally induced effects, the SLP anomalies are reduced in the TA during MAM.

The associated warm composites of the 200 hPa ψ anomalies show three dipolar structures straddling the equatorial latitudes (Figure 15(a) and (b)) similar to those in Figure 4(a) and (b). The Rossby wave patterns here are relatively weaker than those previously discussed, in particular during MAM. This is consistent with

Copyright © 2006 Royal Meteorological Society

DOI: 10.1002/joc

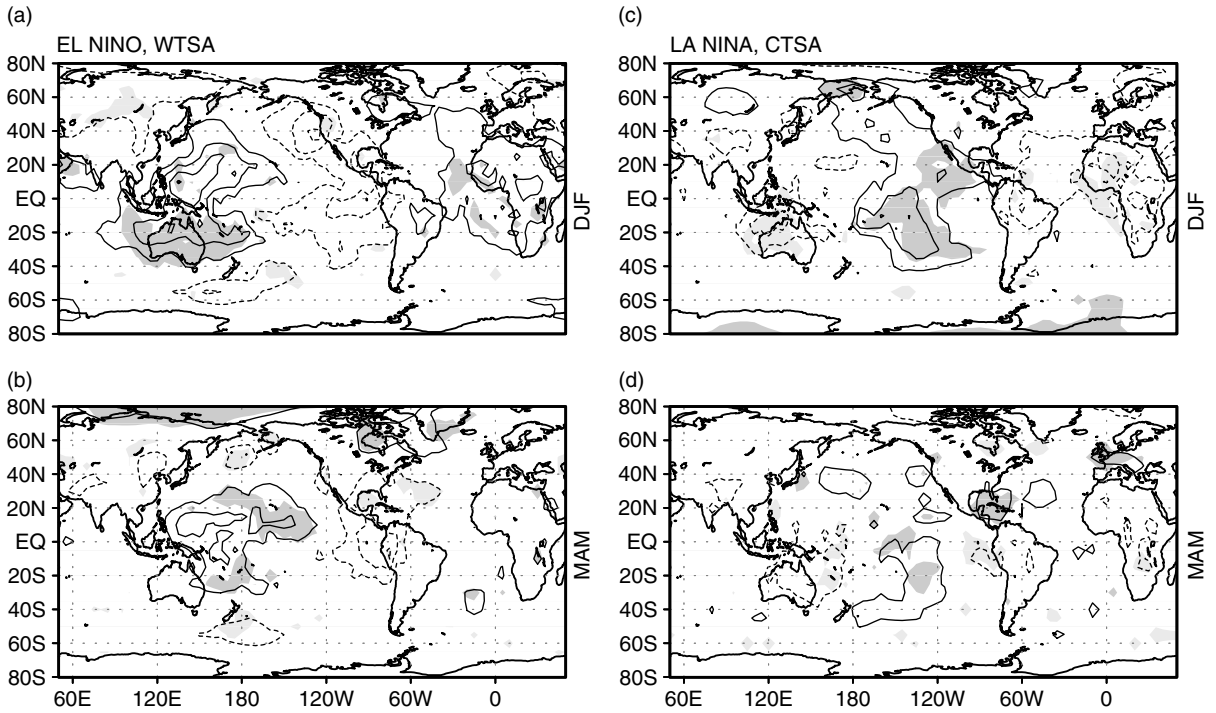

Figure 14. Mean standardized SLP anomalies for El Niño and WTSA during (a) DJF and (b) MAM; mean standardized SLP anomalies for La Niña and CTSA during (c) DJF and (d) MAM. Display is the same as that in Figure 3. Shaded area encompasses significant values at the 95% confidence level

the small amplitude of the associated SST anomalies in the eastern tropical Pacific and with the southward cross equatorial SST gradient in the TA (Figure 13(b)). The SST patterns in the eastern equatorial Pacific and in the TSA independently have opposite effects on the NEB rainfall. The rainfall anomalies for El Niño and WTSA conditions are negative during DJF and MAM, with significant values during DJF. This means that the eastern equatorial Pacific conditions are dominant. The rainfall anomalies in the case of El Niño and WTSA show smaller magnitudes than those in the case of El Niño and NTSA, in particular during MAM (Figures 16(a), (b), 7(a) and (b)). So, for the El Niño and WTSA situation, the warm waters in TSA act to reduce the amplitude of El Niño related negative rainfall anomalies.

The cold composites of the 200 hPa ψ anomalies (Figure 15(c) and (d)) show smaller magnitudes than those depicted in Figure 4(c) and (d). Again, this might also result from the competing effects of the SST patterns in the eastern tropical Pacific and in the TSA (Figure 13(c) and (d)). The associated NEB rainfall composites show quite pronounced anomalies, in particular during MAM (Figure 16(c) and (d)). This might be explained by the weakening of negative SST anomalies in the eastern equatorial Pacific from DJF to MAM while the negative SST anomalies in the TSA remain quite strong. In consequence, the negative TSA anomalies overwhelm the La Niña teleconnections in the TA and over NEB, inhibiting convection and thus causing drought over the northern sector of the NEB (Figure 16(c) and (d)). Previous papers have consistently provided indications that the SST anomalies in TA precondition the ENSO teleconnections in NEB (Giannini *et al*., 2004; Kayano and Andreoli, 2006).

Comparisons between the El Niño and WTSA and the El Niño and NTSA cases, and between the La Niña and CTSA and the La Niña and NTSA cases suggest that the TSA influence is larger in the case of La Niña than in El Niño. This result is consistent with the findings of Pezzi and Cavalcanti (2001) who showed that during La Nina events the Atlantic Ocean conditions have a larger effect on the precipitation over NEB than the Pacific Ocean conditions.

Copyright © 2006 Royal Meteorological Society

DOI: 10.1002/joc

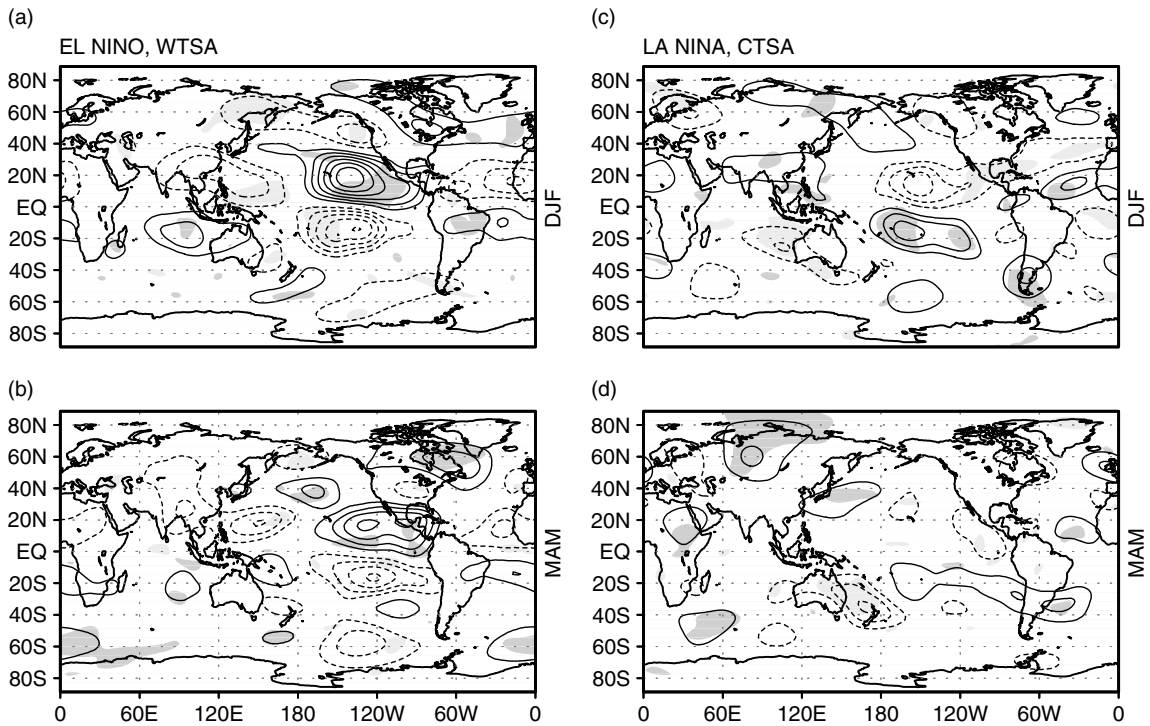

Figure 15. Composites of the 200 hPa ψ anomalies for El Niño and WTSA during (a) DJF and (b) MAM; composites of the 200 hPa ψ anomalies for La Niña and CTSA during (c) DJF and (d) MAM. Display is the same as that in Figure 4. Shaded area encompasses significant values at the 95% confidence level

4. CONCLUSIONS

This paper reexamines the relative role of the tropical Pacific and the TSA on the rainfall over NEB. This has been done by isolating the ENSO-related patterns from the TSA-related anomalous patterns for SST, SLP, 925 hPa wind, 200 hPa ψ, 500 hPa ω, and for the NEB rainfall. These patterns are then compared to the combined ENSO- and TSA-related patterns to infer the relative importance of the tropical Pacific and the TSA on the rainfall over NEB. Analyses are done for austral summer (DJF) and autumn (MAM) seasons.

Previous papers have pointed out two ways in which ENSO extremes relate to the NEB rainfall variability: one is a direct mechanism through an ENSO-related anomalous Walker circulation that influences the Atlantic ITCZ positioning (Saravanan and Chang, 2000; Giannini *et al*., 2001; Chiang *et al*., 2000); the other is through an indirect mechanism via the midlatitude atmospheric bridge similar to the PNA pattern, which affects the TNA SST anomalies, altering the ITCZ positioning (e.g. Nobre and Shukla, 1996). In the present analyses, the composites of several variables for ENSO extremes and TSA neutral conditions provide indications that both mechanisms might act to cause ENSO-related rainfall variability in NEB. The difficulties to isolate these mechanisms from the observational analyses are due to the fact that both mechanisms seem to be active during ENSO extremes (Dai and Wigley, 2000).

Under ENSO neutral conditions, the isolated effect of the TSA SST variability on the NEB rainfall is more pronounced and statistically more significant for the WTSA during MAM. In this case, the SST anomalies in the TSA are responsible for the anomalous positioning of the ITCZ, which affects the NEB rainfall. The seasonal differences in the low-level anomalous winds explain the seasonal differences in the rainfall fields (Figure 11(a)). For the WTSA composite, the intensified northwesterlies in the equatorial TA maintain the ITCZ to the south of its normal position until MAM, favoring the positive NEB rainfall anomalies (Figure 12(b)). For the CTSA composite, the intensified southeasterlies during DJF inhibit the southward displacement of the ITCZ, thus causing reduced rainfall over NEB.

Copyright © 2006 Royal Meteorological Society

DOI: 10.1002/joc

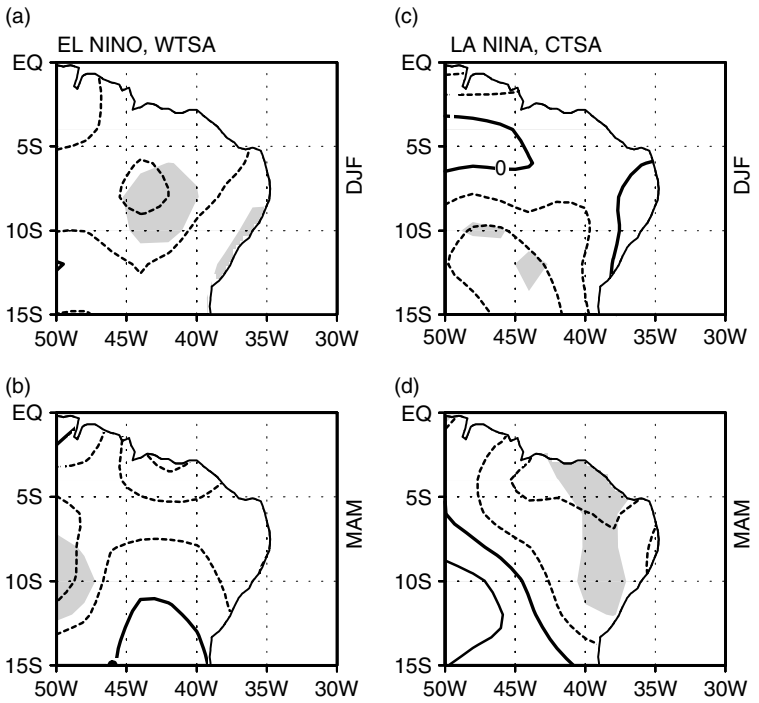

Figure 16. Mean standardized rainfall anomalies for El Niño and WTSA during (a) DJF and (b) MAM; mean standardized rainfall anomalies for La Niña and CTSA during (c) DJF and (d) MAM. Display is the same as that in Figure 7. Shaded area encompasses significant values at the 90% confidence level

The combined effect of tropical Pacific and TSA SST anomalies on the NEB rainfall variability has been examined considering the same SST conditions in both basins (warm or cold). These cases refer to El Niño and WTSA composite (warm composite) and to La Niña and CTSA (cold composite). For both composites, the SST anomalies in the tropical Pacific and in the TA have opposite effects on the NEB rainfall. In fact, the El Niño (La Niña) favors dry (wet) conditions in NEB while the WTSA (CTSA) favors wet (dry) conditions in this region (Kousky *et al*., 1984; Kayano *et al*., 1988; Hastenrath and Heller, 1977; Moura and Shukla, 1981; Nobre and Shukla, 1996). Therefore, the anomalous patterns of the analyzed variables for the same SST conditions in the tropical Pacific and TSA (Figures 13, 14, 15 and 16) are weaker than the corresponding ones for composites of ENSO extremes and NTSA conditions. Furthermore, the NEB rainfall anomaly composites for La Niña and CTSA feature negative anomalies in the northern sector of NEB, which show large significant magnitudes during MAM. In this case, the local SST variability in the TSA is the dominant forcing to the NEB rainfall variability. Thus, the results presented here confirm previous findings that the SST anomalies in the TSA might precondition ENSO teleconnections in the TA region (Giannini *et al*., 2004). Therefore, in some situations the tropical Pacific may have a secondary influence on the NEB rainfall variability while the TSA determines the climate variability in this region. Hence, the monitoring of the SST anomalies over TSA is essential for climate forecasting purposes in this region.

ACKNOWLEDGEMENTS

The authors are grateful to the two anonymous reviewers for their useful comments. The first author was supported by the Conselho Nacional de Desenvolvimento Científico and Tecnológico (CNPq) of Brazil under the project number PD-150.151/04-7. The second author was partially supported by CNPq. The authors are also grateful to Dr Mike Hulme for the provision of the 'gu23wld0098.dat' (version 1.0) constructed at the Climatic Research Unit, University of East Anglia, Norwich, UK. The NCEP Reanalysis data was

Copyright © 2006 Royal Meteorological Society

DOI: 10.1002/joc

provided by the NOAA-CIRES Climate Diagnostics Center, Boulder, Colorado, USA, from the web site at http://www.cdc.noaa.gov/.

REFERENCES

Chang P, Ji L, Li H. 1997. A decadal climate variation in the tropical Atlantic ocean from thermodynamic air-sea interactions. *Nature* **385**: 516–518.

Chiang JCH, Kushnir Y, Zebiak SE. 2000. Interdecadal changes in eastern Pacific ITCZ variability and its influence on the Atlantic ITCZ. *Geophysical Research Letters* **27**: 3687–3690.

Covey DC, Hastenrath S. 1978. The Pacific El Niño phenomenon and the Atlantic circulation. *Monthly Weather Review* **106**: 1280–1287.

Curtis S, Hastenrath S. 1995. Forcing of anomalous sea surface temperature evolution in the tropical Atlantic during Pacific warm events. *Journal of Geophysical Research* **100**: 15835–15847.

Dai AG, Wigley TML. 2000. Global patterns of ENSO-induced precipitation. *Geophysical Research Letters* **27**: 1283–1286.

Enfield DB, Mayer DA. 1997. Tropical Atlantic SST variability and its relation to El Niño-Southern Oscillation. *Journal of Geophysical Research* **102**: 929–945.

Giannini A, Saravanan R, Chang P. 2004. The preconditioning role of tropical Atlantic variability in the development of the ENSO teleconnection: implications for the prediction of Nordeste rainfall. *Climate Dynamics* **22**: 839–855, DOI: 10.1007/s00382-004-0420-2.

Giannini A, Chiang JCH, Cane MA, Kushnir Y, Seager R. 2001. The ENSO teleconnection to the tropical Atlantic Ocean: contributions of the remote ans local SSTs to rainfall variability in the tropical Americas. *Journal of Climate* **14**: 4530–4544.

Hastenrath S. 1976. Variations in low-latitude circulation and extreme climatic events in the tropical Americas. *Journal of the Atmospheric Sciences* **33**: 202–215.

Hastenrath S. 1990. Prediction of Northeast Brazil rainfall anomalies. *Journal of Climate* **3**: 893–904.

Hastenrath S, Greischar L. 1993. Further work on the prediction of Northeast Brazil rainfall anomalies. *Journal of Climate* **6**: 743–758.

Hastenrath S, Heller L. 1977. Dynamics of climatic hazards in northeast Brazil. *Quarterly Journal of the Royal Meteorological Society* **103**: 77–92.

Horel JD, Wallace JM. 1981. Planetary scale atmospheric phenomena associated with the Southern Oscillation. *Monthly Weather Review* **109**: 813–829.

Hulme MA. 1992. 1951–1980 global land precipitation climatology for the evaluation of general circulation models. *Climate Dynamics* **7**: 57–72.

Hulme MA. 1994. Validation of large-scale precipitation fields in general circulation models. In *Global Precipitations and Climate Change*, Desbois M, Desalmand F (eds). *NATO ASI series*. Springer-Verlag: Berlin; 466.

Hulme MA, Osborn TJ, Johns TC. 1998. Precipitation sensitivity to global warming: comparison of observations with HadCM2 simulations. *Geophysical Research Letters* **25**: 3379–3382.

Kalnay E, Kanamitsu M, Kistler R, Collins W, Deaven D, Gandin L, Iredell M, Saha S, White G, Woollen J, Zhu Y, Chelliah M, Ebisuzaki W, Higgins W, Janowiak J, Mo KC, Ropelewski C, Wang J, Leetmaa A, Reynolds R, Jenne R, Joseph D. 1996. The NCEP/NCAR 40-year reanalysis project. *Bulletin of the American Meteorological Society* **77**: 437–471.

Kane RP. 1992. El Niño and la Niña events and rainfall in NE and South Brazil. *Revista Brasileira de Geofísica* **10**: 49–59.

Kayano MT, Andreoli RV. 1998. Interanual variability of the upper tropospheric circulation. *Meteorology and Atmospheric Physics* **68**: 143–150.

Kayano MT, Andreoli RV. 2006. Relationships between rainfall anomalies over Northeastern Brazil and the El Niño-Southern Oscillation. *Journal of Geophysical Research* (in press).

Kayano MT, Kousky VE. 1993. An index of low-frequency variability in the global tropics. In *Proceedings of the Seventeenth Annual Climate Diagnostics Workshop*, Norman, Oklahoma, 341–347.

Kayano MT, Rao VB, Moura AD. 1988. Tropical circulations and the associated rainfall anomalies during two contrasting years. *Journal of Climatology* **8**: 477–488.

Kiladis G, Diaz HF. 1989. Global climatic anomalies associated with extremes in the Southern Oscillation. *Journal of Climate* **2**: 1069–1090.

Kousky VE, Kayano MT, Cavalcanti IFA. 1984. A review of the Southern Oscillation: oceanic-atmospheric circulation changes and related rainfall anomalies. *Tellus* **36A**: 490–504.

Mo KC. 2000. Relationships between low-frequency variability in Southern Hemisphere and sea surface temperature anomalies. *Journal of Climate* **13**: 3599–3610.

Mo KC, Nogués-Paegle J. 2001. The Pacific-South American modes and their downstream effects. *International Journal of Climatology* **21**: 1211–1229.

Moura A, Shukla J. 1981. On the dynamics of droughts in Northeast Brazil: observations, theory, and numerical experiments with a general circulation model. *Journal of the Atmospheric Sciences* **38**: 2653–2675.

Nobre P, Shukla J. 1996. Variations of sea surface temperature, wind stress, and rainfall over the tropical Atlantic and South America. *Journal of Climate* **9**: 2464–2479.

Panofsky HA, Brier GW. 1968. *Some Applications of Statistics to Meteorology*. Pennsylvania State University: University Park, PA; 224 pp.

Pezzi LP, Cavalcanti JFA. 2001. The relative importance of ENSO and tropical Atlantic sea surface temperature anomalies for seasonal precipitation over South America: a numerical study. *Climate Dynamics* **17**: 205–212.

Rasmusson EM, Carpenter TH. 1982. Variations in tropical sea surface temperature and wind surface fields associated with the Southern Oscillation/El Niño. *Monthly Weather Review* **110**: 354–384.

Ropelewski CF, Halpert MS. 1987. Global and regional scale precipitation patterns associated with the El Niño/Southern Oscillation. *Monthly Weather Review* **115**: 1606–1626.

Ropelewski CF, Halpert MS. 1989. Precipitation patterns associated with the high index phase of the Southern Oscillation. *Journal of Climate* **2**: 268–284.

Copyright © 2006 Royal Meteorological Society

Saravanan R, Chang P. 2000. Interaction between tropical Atlantic variability and El Niño-Southern Oscillation. *Journal of Climate* **13**: 2177–2194.
Seager R, Kushnir Y, Naik N, Miller J, Chang P, Hazeleger W. 2001. Looking for the role of the ocean in tropical Atlantic decadal climate variability. *Journal of Climate* **14**: 638–655.
Servain J. 1991. Simple climatic indices for the tropical Atlantic Ocean and some applications. *Journal of Geophysical Research* **96**: 15137–15146.
Smith TM, Reynolds RW. 2003. Extended reconstruction of global sea surface temperatures based on COADS data (1854–1997). *Journal of Climate* **16**: 1495–1510.

Copyright © 2006 Royal Meteorological Society

DOI: 10.1002/joc